Dendritic to non-dendritic transitions in Au islands investigated by scanning tunneling microscopy and Monte Carlo simulations

Shohei Ogura,[1,*] Katsuyuki Fukutani,[1] Masuaki Matsumoto,[1] Tatsuo Okano,[1] Michio Okada,[2] and Takaaki Kawamura[3]
[1]*Institute of Industrial Science, University of Tokyo, 4-6-1 Komaba, Meguro-ku, Tokyo 153-8505, Japan*
[2]*Department of Chemistry, Graduate School of Science, Osaka University, 1-1 Machikaneyama-cho, Toyonaka, Osaka 560-0043, Japan*
[3]*Department of Mathematics and Physics, Yamanashi University, 4-3-11 Takeda, Kofu 400-8511, Japan*
(Received 21 November 2005; revised manuscript received 13 February 2006; published 30 March 2006)

We investigated the structures of the two-dimensional Au islands grown on Ir(111) and Pt(111) using scanning tunneling microscopy and Monte Carlo simulations. We found that the Au islands have dendritic, triangularly compact, and irregularly compact shapes depending on the underlying substrate. We also found a strong layer dependence of the island density. Monte Carlo simulation results demonstrate that the fractal dimensions of these dendritic islands are determined by competition between terrace diffusion and edge diffusion of adatoms. Furthermore, the fractal dimension changes continuously from about 1.7 to 2 as a function of the edge diffusion barrier, which is discussed on the basis of the generalized diffusion limited aggregation model.

DOI: 10.1103/PhysRevB.73.125442 PACS number(s): 68.55.Ac, 68.70.+w

I. INTRODUCTION

Metals grown on a substrate reveal a variety of shape on a nanoscale, e.g., three-dimensional island, two-dimensional thin layer, dendrite, etc. An interesting growth mode is dendritic growth which has been studied both experimentally and theoretically. The formation mechanism of dendritic islands is known to be diffusion limited aggregation (DLA).[1] In the DLA model, an atom is released on a surface and it randomly diffuses until it arrives at an edge site of an existing island. After repeated cycles of release, diffusion, and aggregation of atoms, the islands formed in the mechanism show a randomly ramified shape. Such dendritic islands are known to have fractal properties. They possess the property of self-similarity with a fractal dimension of about 1.7.[1–3] Experimental dendritic growth is observed on some metal-on-metal systems with scanning tunneling microscopy (STM): For example, Au on Ru(0001) (Ref. 4) and Pt on Ru(0001) (Refs. 5 and 6) at room temperature, and Ag on Pt(111) (Ref. 7) at a low temperature of 110 K. On the other hand, it is known that an island shape strongly depends on the growth condition, especially sample temperature and deposition rate. As a temperature dependence of the island shape, gradual transition from dendritic islands to compact islands with increasing sample temperature has been reported.[8–14] Although the adatom diffusion from in-layer twofold coordinated sites of island edges[15] are reported to play an important role in the transition,[8–12] a detailed mechanism has not been discussed and an understanding of how the fractal dimension changes in terms of statistical physics is lacking.

Such a variety of island shape is related to their surface chemical reactivities. Recently, Au has been reported to have particular chemical reactivities depending on its shape. Whereas a bulk-Au surface is known to be inert, Au nanoparticles have particular chemical reactivities for CO oxidation,[16] and Au films have anomalous reactivities for hydrogen dissociative adsorption.[17–20] Furthermore, previous studies revealed that the significantly high density of edge atoms of dendritic islands is attributed to a particular chemical property.[21,22] Therefore, the ability to control the density of edge atoms would make a substantial contribution to the improvement of catalytic activities. Our final goal is to relate the nanoshape of Au with its reactivity and tailor surfaces having desirable reactivities by controlling the island shape. For these purposes, it is necessary to investigate mechanisms of film growth. The motivation behind the present work is thus to elucidate the mechanism of the Au film growth and understand the atomic processes that determine the island shapes.

In this paper, we report a study on the structures of two-dimensional Au islands grown on Ir(111) and Pt(111) using STM. We demonstrate that Au islands have dendritic, triangularly compact, and irregularly compact shapes depending on the underlying substrate. We also found a layer dependence of density of terrace islands. We performed Monte Carlo simulations in order to elucidate the origin of the difference in the island shape, and found that the fractal dimension representing the island compactness strongly depends on the energy barrier for adatom diffusion from twofold coordinated sites of the island edges. Furthermore, the fractal dimension of the islands gradually changes from 1.7 to 2 as the diffusion barrier decreases. We discuss the origin of the continuous change of the fractal dimension on the basis of the generalized DLA model.[23,24]

II. EXPERIMENT

The STM measurements were performed in an ultra-high vacuum (UHV) chamber equipped with a four-grid optics for low-energy electron diffraction (LEED) and Auger electron spectroscopy (AES), and a variable-temperature STM (OMICRON VT-AFM/STM). The base pressure was typically 1×10^{-9} Pa. The Ir and Pt crystals have a size of 3

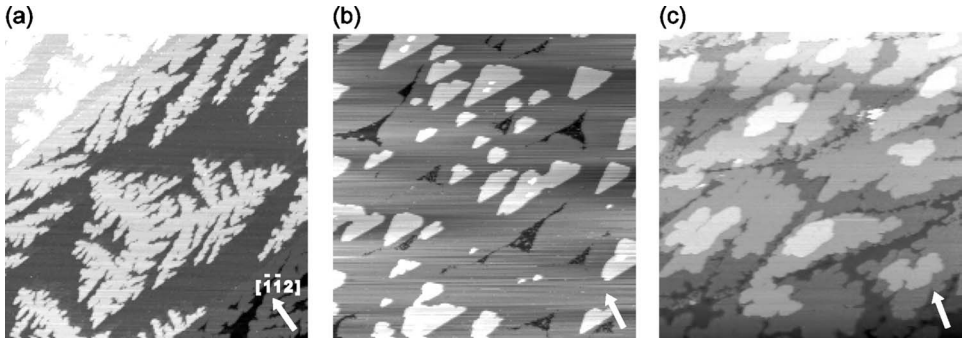

FIG. 1. STM topographic images (500×500 nm^2) of (a) 0.52 ML, (b) 1.2 ML, and (c) 3.6 ML Au deposited on Ir(111) at room temperature. Images were taken at sample currents and voltages of (a) 0.19 nA and 0.15 V, (b) 0.21 nA and 0.14 V, and (c) 0.19 nA and 0.17 V. Arrows in the figure denote the [$\bar{1}\bar{1}$2] direction.

$\times 3$ mm^2 and are oriented in the (111) direction with an accuracy of $\pm 0.1°$. The average terrace width measured by STM was wider than 200 nm on both surfaces and each terrace is separated by monoatomically high steps. The Ir(111) and Pt(111) surfaces were cleaned by successive cycles of Ar^+ ion bombardment at 500 eV, heating at 1100 K in 7×10^{-6} Pa O_2 atmosphere, and final flashing at 1400–1500 K. The surface cleanliness was checked by LEED, AES, and STM. Deposition of Au was conducted using heated tungsten coils loaded with a Au wire at a rate of 1×10^{-3} monolayer (ML) s^{-1} [1 ML$=1.57\times10^{15}$ atoms cm^{-2} for Ir(111) and 1.50×10^{15} atoms cm^{-2} for Pt(111)] and a sample temperature of 300 K. The deposited amount of Au atoms was monitored by a quartz oscillator placed near the sample during deposition, and the exact coverage was estimated from the STM images. After STM measurements of a sample surface at 300 K, the surface was recleaned and a new Au layer was prepared on the clean surface. The STM data were recorded in the constant-current mode, with tunneling currents around 0.2 nA and sample bias voltages in the range of −0.2 to +0.2 V. All STM images in the present paper are displayed as topographic topviews with a size of 500×500 nm^2 with higher areas denoted by brighter images.

III. RESULTS

Figure 1 shows STM images of the Au islands grown on Ir(111) at three coverages of 0.52, 1.2, and 3.6 ML. Below one monolayer, two-dimensional dendritic islands with monoatomic height of Au are formed on terraces and at ascending step edges as shown in Fig. 1(a). The Au islands on terraces have a triangular envelope and their branches preferentially grow into three $\langle\bar{1}\bar{1}2\rangle$ directions rotated by 120° with respect to each other, which reflects the threefold symmetry of the Ir(111) substrate. The Au islands growing from the Ir steps can be clearly distinguished from the Ir step edges due to the height difference of 0.014 nm between Au and Ir. Their branches are growing in the same direction as the main branches of the terrace islands. The average length and width of the main branches of the terrace islands are about 250 and 30 nm, respectively. From the STM images taken at several spots, the average island density on the terrace is estimated to be 4 ± 1 μm^{-2}. The island density in the present paper is calculated by dividing the number of islands in an image by the total area of the image. No nucleation of the second-layer islands is observed on the first-layer islands at this coverage, indicating that atoms deposited directly on an existing island can descend easily from the island, i.e., the energy barrier is sufficiently low for adatoms to descend from the first-layer island.

Increasing Au coverage above one monolayer results in a change in the shape and density of the terrace island. In contrast to the first-layer islands, as shown in Fig. 1(b), the second-layer islands have a triangularly compact shape with a size of about 60 nm, which still reflects the threefold symmetry of the Ir(111) substrate. The triangle corners of the second-layer islands are pointing to the $\langle\bar{1}\bar{1}2\rangle$ directions, which indicates that the second-layer islands grow into the same direction as that of the first-layer islands. Between these islands, there are triangular indentations with a size of about 50 nm whose corners are pointing to the $\langle11\bar{2}\rangle$ directions rotated by 60° with respect to the $\langle\bar{1}\bar{1}2\rangle$ directions. These indentations are remnants of coalescence of the first-layer dendritic islands, since such triangular indentations are also found in Fig. 1(a) where the islands growing in different directions from a step run across each other. From the height distribution of the image, 96% of the Ir substrate surface is covered by Au. The density of the second-layer island is 140 ± 25 μm^{-2}, which is much higher than that of the first-layer island. The result suggests that Au atoms on the first Au layer grown on Ir are less mobile than on the bare Ir surface, since a higher island density corresponds to a shorter diffusion length of adatoms under a condition of the constant flux and the constant sample temperature.[25] In spite of the shorter diffusion length of Au adatoms on the first Au layer than on the bare Ir surface, nucleation of the second-layer island only starts after the first-layer growth is almost completed, which can be attributed to the dendritic growth of the first layer. Since such dendritic islands have much space between their branches, atoms deposited directly on the island can easily reach the edge sites of the island after short diffusion and descend from the island. As a result, the probability of the nucleation of the second-layer island is largely suppressed making the first layer almost completely flat.

Further increasing Au coverage up to 3.6 ML leads to formation of irregularly shaped compact islands as shown in Fig. 1(c). The top-layer islands in the image are the fifth-layer islands with a size of about 100 nm in diameter. With a closer look at the island shape, the contour of the fifth-layer islands is found to have a hexagonal shape. Such an irregularly compact shape is observed from the third-layer islands. Analysis of the height distribution shows that less than 0.4% of the area is substrate Ir, which is consistent with the previous AES measurements.[17]

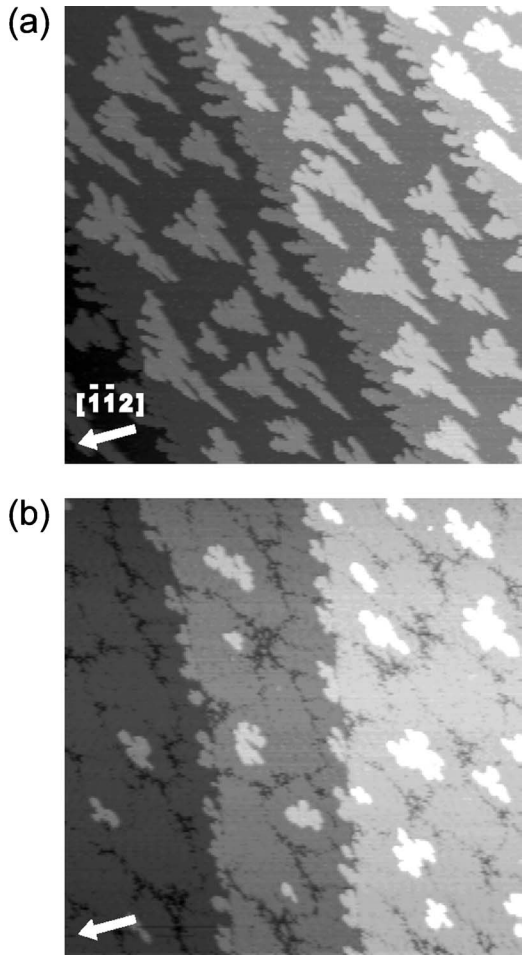

FIG. 2. STM topographic images (500×500 nm^2) of (a) 0.37 ML and (b) 1.0 ML Au deposited on Pt(111) at room temperature. Images were taken at a sample current of 0.15 nA and a voltage of −0.14 V. Arrows in the figure denote the $[\bar{1}\bar{1}2]$ direction.

Figure 2 shows STM images of the Au islands grown on Pt(111). As on Ir, the first-layer islands on Pt also have a two-dimensional dendritic shape with a triangular envelope after 0.37 ML Au deposition as shown in Fig. 2(a). The branches are also growing in the $\langle\bar{1}\bar{1}2\rangle$ directions. The average length and width of the main branches of the terrace islands are about 60 and 20 nm, respectively. Although the first-layer islands have a dendritic shape with a triangular envelope on both Ir and Pt, the compactness and density of the dendritic islands are different between these substrates. The first-layer islands on Pt are more compact than those on Ir, and the density of the first-layer islands on Pt is 115 ± 20 μm^{-2}, which is much higher than that on Ir. The difference in the compactness and island density will be discussed in more detail below.

Figure 2(b) shows a STM image taken after 1.0 ML Au deposition on Pt. The second-layer islands on Pt have an irregularly compact shape with a size of about 50 nm, whereas the second-layer islands on Ir have a triangularly compact shape [Fig. 1(b)]. There are some indentations recognized in the image, which are generated by coalescence of the dendritic islands. The higher indentation density compared with that on Ir [Fig. 1(b)] reflects the higher density of the first-layer islands. From the height distribution of the image, 94% of the Pt substrate surface is covered by Au. The density of the second-layer islands on Pt is 95 ± 10 μm^{-2}, which is similar to that of the first-layer islands on Pt.

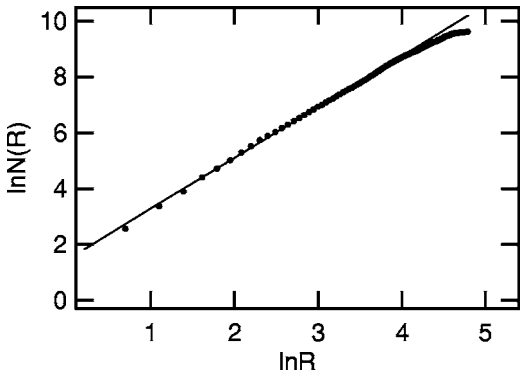

FIG. 3. An example of a mass-radius relation calculated on a first-layer Au island grown on Ir(111). The fractal dimension obtained by fitting a straight line to the data is 1.82.

In order to quantify the compactness of the islands observed on each layer, we evaluated the fractal dimension d_f of the islands by the mass-radius relation method.[26] In this method, a circle with radius R is put at the center of an island and the number of atoms $N(R)$ in the circle is counted as a function of R. $N(R)$ is known to have a power law form $N(R)\sim R^{d_f}$ over a range of R from a few atomic distances to the size of the island. Figure 3 shows a typical result obtained by the method for a first-layer island grown on Ir. From the slope of the straight line fitted to the data in the scaling regime on double logarithmic plot $\ln N(R)$ versus $\ln R$, we obtain the fractal dimension of 1.82. The average fractal dimensions of the islands obtained from several STM images on each layer are compiled in Table I with their island shapes and densities. The average fractal dimension of the first-layer islands is 1.81 ± 0.02 on Ir and 1.92 ± 0.02 on Pt. On the other hand, the second- or higher-layer islands on both substrates have a fractal dimension of 2. These results clearly show a layer dependence of the fractal dimension.

IV. SIMULATION

Our STM results revealed that the shape, density, and fractal dimension of the Au islands strongly depend on the

TABLE I. Shape, fractal dimension, and density of the islands obtained on each layer by STM measurements. The fractal dimensions are analyzed by the mass-radius relation method.

Layer	Shape	Fractal dimension	Density (μm^{-2})
First on Ir	Dendritic	1.81±0.02	4±1
Second on Ir	Triangular	2	140±25
Fifth on Ir	Irregular	2	45±10
First on Pt	Dendritic	1.92±0.02	115±20
Second on Pt	Irregular	2	95±10

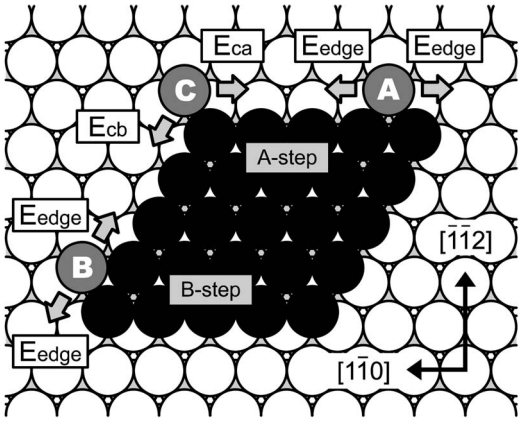

FIG. 4. Illustration of the diffusion processes along island edges and corresponding energy barriers considered in the simulation. Black circles represent island atoms and gray circles labeled A, B, and C represent edge atoms at a twofold site of the A step, at a twofold site of the B step and at a onefold corner site, respectively.

underlying substrate. In order to elucidate the growth mechanism of the islands, i.e., decisive factors for the island shape, density, and fractal dimension, we performed kinetic Monte Carlo simulations based on the DLA model with diffusion along island edges taken into consideration. We consider a fcc(111) surface shown in Fig. 4 where we distinguish between A and B steps inherent in the islands grown on the fcc(111) surface:[27] A steps are {100} facets, and B steps are {111} facets. The $\langle\bar{1}\bar{1}2\rangle$ and $\langle 11\bar{2}\rangle$ directions are perpendicular to the A and B steps, respectively. In the simulation, atoms are put on this substrate randomly at a rate of F ML s^{-1} and allowed to diffuse thermally on the surface to form islands. Adsorption sites are assumed to be only the normal fcc hollow sites and the difference in the lattice constant between the adsorbed atom and the substrate atom is not taken into account. A terrace adatom diffuses to the nearest-neighbor fcc hollow sites at a rate of $\nu_t = \nu_0 \exp(-E_t/kT)$, where ν_0 is an attempt frequency, E_t is a terrace diffusion barrier, k is the Boltzmann constant, and T is a sample temperature. We assume that adatoms at one or twofold coordinated sites of islands are still mobile along the island edges until they come to threefold or higher coordinated sites. This means that we consider *corner* and *edge* diffusions[28] in addition to terrace diffusion: The corner diffusion is the diffusion from the onefold coordinated corner sites to neighboring steps, and the edge diffusion is the diffusion from the twofold coordinated sites to n-fold coordinated sites ($n \geq 1$). Since the corner diffusion barrier is known to be different for the A and the B steps,[28–31] we distinguish these two corner diffusions. Figure 4 illustrates the diffusion processes and their diffusion barriers at an island considered in our simulations: E_{ca} and E_{cb} are the diffusion barriers of corner diffusion to the A and B steps, respectively, and E_{edge} corresponds to the edge diffusion barrier. The corner and edge diffusion processes occur at a rate of $\nu_0 \exp(-E_i/kT)$, where E_i represents respective diffusion barrier and the attempt frequency ν_0 is assumed to be the same for all diffusion processes. Detachment of the edge atoms from the islands is neglected. When atoms are deposited on an existing island, they are forced to diffuse on the island preferentially until they descend from the island and become edge atoms. All simulations are performed under the same condition as the experiments, $T=300$ K and $F=1\times10^{-3}$ ML s^{-1}.

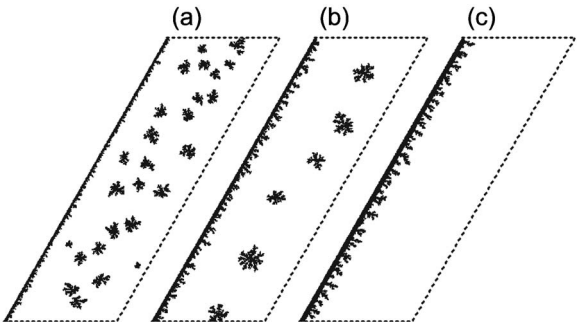

FIG. 5. Monte Carlo simulations (2130×740 lattice sites) in the case of $\nu_c=\nu_t$ at three ν_t's of (a) 3.0×10^{10} s^{-1}, (b) 5.5×10^{11} s^{-1}, (c) 6.8×10^{12} s^{-1} under the condition of $T=300$ K and $F=1\times10^{-3}$ ML s^{-1}. The coverage is 0.06 ML (9×10^4 atoms).

First, we evaluate the terrace diffusion rate on each layer from the experimental values of the island density shown in Table I by comparing with the simulation results. For this purpose, we consider a fcc(111) surface with 2130×740 lattice sites. On the left side of the surface, we place an array of atoms representing an ascending A step which acts as a trap site for adatoms, and apply a periodic boundary condition to the surface. The lattice size corresponds to a typical terrace width of 200 nm for Ir(111) observed in our STM images. We assume that the adatoms coming from the left side due to the periodic boundary condition can descend the step and attach to it. We also assume that the adatoms can diffuse over the boundary between the step and the islands growing from the step, since the adatoms do not accumulate at such boundaries as shown in Figs. 1(a) and 2(a). Since E_{edge} has little effect on the island density, we take account of only E_t, E_{ca}, and E_{cb}. Under this condition, dimers as well as monomers can diffuse on the surface through a succession of corner diffusion.

Figure 5 shows the simulation results under the condition

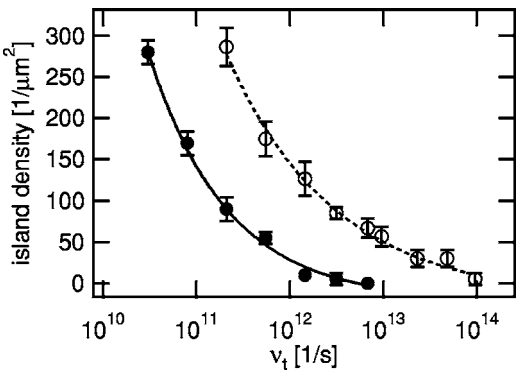

FIG. 6. Island density obtained from the simulations as a function of ν_t under the condition of $T=300$ K and $F=1\times10^{-3}$ ML s^{-1}. Filled circles represent the island densities under the condition of $\nu_c=\nu_t$. Open circles represent the island densities without corner diffusion.

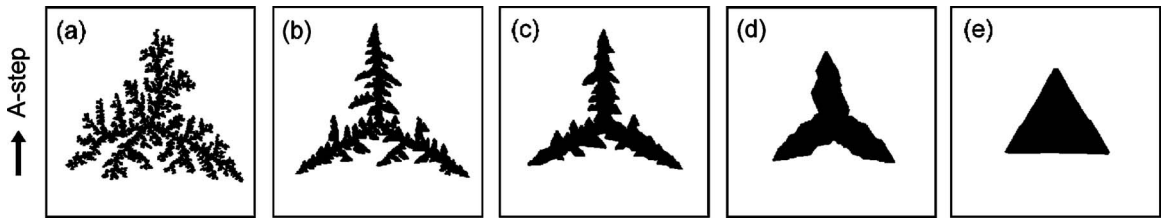

FIG. 7. Images of island shapes (400×460 lattice sites) obtained by Monte Carlo simulations as a function of E_{edge}: (a) 0.85 eV, (b) 0.58 eV, (c) 0.50 eV, (d) 0.40 eV, and (e) 0.25 eV. The number of atoms is 20 000. Calculations were performed under the condition of $E_t=0.010$ eV, $E_{ca}=0.10$ eV, $E_{cb}=0.25$ eV, $T=300$ K, and $F=1\times10^{-3}$ ML s^{-1}. The arrow in the figure denotes the direction perpendicular to the A step.

of $\nu_c=\nu_t$, where ν_c is the corner diffusion rate. The number of deposited atoms is 90 000, which corresponds to 0.06 ML. The island density is found to saturate at this coverage in the simulations. As ν_t becomes larger, the density of terrace islands becomes smaller, and finally all adatoms attach to the step without forming isolated terrace islands [Fig. 5(c)]. Figure 6 shows the island density obtained by the simulations as a function of ν_t. The open circles represent the results under the condition of no corner diffusion where dimers are stable and immobile. The values correspond to an upper bound for the island density because the dimer diffusion, which is caused by the corner diffusion, reduces the island density. The filled circles represent the results under the condition of $\nu_c=\nu_t$. The data corresponds to a lower bound for the island density because the corner diffusion rate would be lower than the monomer diffusion rate. With an island density given, the terrace diffusion rate therefore is expected to lie between the two curves shown in Fig. 6. Compared to the experimental island densities listed in Table I, the terrace diffusion rates ν_t of Au adatoms on Ir and Pt are estimated to be in the range of 3×10^{12} to 1×10^{14} s^{-1}, and 2×10^{11} to 3×10^{12} s^{-1}, respectively. Assuming that the attempt frequency $\nu_0=1\times10^{13}$ s^{-1} on both substrates, the terrace diffusion barrier E_t for adatoms is lower than 0.04 eV on Ir and in the range of 0.04 to 0.10 eV on Pt. On the other hand, ν_t of Au adatoms on the first Au layer on Ir is estimated to be in the range of 1×10^{11} to 1×10^{12} s^{-1}, i.e., E_t is in the range of 0.06 to 0.12 eV on the assumption of $\nu_0=1\times10^{13}$ s^{-1}. Since the island density is similar on the first Au layer on Pt, the diffusion barrier is also expected to be in the same range.

Next, we investigated how edge diffusion affects the island shape. For this purpose, we consider a fcc(111) surface with 400×460 lattice sites [$\sim110\times110$ nm^2 for Ir(111)], and take account of the edge diffusion from the twofold coordinated sites (E_{edge}) shown in Fig. 4. Initially, seven atoms are placed on the center of the lattice in a hexagonal shape as an immobile seed island. It should be noted that the final island shapes were essentially the same when we start the simulation with one atom as a seed. All simulations were performed under a fixed condition of $E_t=0.010$ eV and $\nu_0=1\times10^{13}$ s^{-1}, which corresponds to the terrace diffusion rate of 6.8×10^{12} s^{-1}. Our simulations revealed that E_t hardly affects the island shape in the range of 0.010 to 0.12 eV, as long as only one island is formed on the terrace.

Figure 7 illustrates the island shapes obtained by the simulations with various values of E_{edge} under the condition of $E_{ca}=0.10$ eV and $E_{cb}=0.25$ eV, i.e., anisotropic corner diffusion. These corner diffusion barriers were set based on the calculated values with the effective medium theory for Ag on Pt(111) where dendritic Ag islands grow into the $\langle\bar{1}\bar{1}2\rangle$ directions.[28] All islands consist of 20 000 atoms, which correspond to 0.11 ML. At $E_{\mathrm{edge}}=0.85$ eV, the island shows a dendritic shape with a triangular envelope as shown in Fig. 7(a). As E_{edge} decreases, on the other hand, the island shape gradually becomes more compact and finally becomes triangular at $E_{\mathrm{edge}}=0.25$ eV as shown in Fig. 7(e). Compared to the experimental results, the island shown in Fig. 7(b) resembles the first-layer islands on Ir [Fig. 1(a)]. The islands shown in Figs. 7(c) and 7(e) resemble the first-layer islands on Pt [Fig. 2(a)] and the second-layer islands on Ir [Fig. 1(b)], respectively. Figure 8 illustrates the simulation results under the condition of isotropic corner diffusion, $E_{ca}=E_{cb}=0.11$ eV. These values are chosen to ensure that the corner diffusion occurs at the same rate as the anisotropic corner diffusion. Similar to the anisotropic case of Fig. 7, the island gradually becomes compact with decreasing E_{edge}. In contrast to Fig. 7, the island shape changes from a randomly ramified shape at $E_{\mathrm{edge}}=0.80$ eV to a hexagonal one at

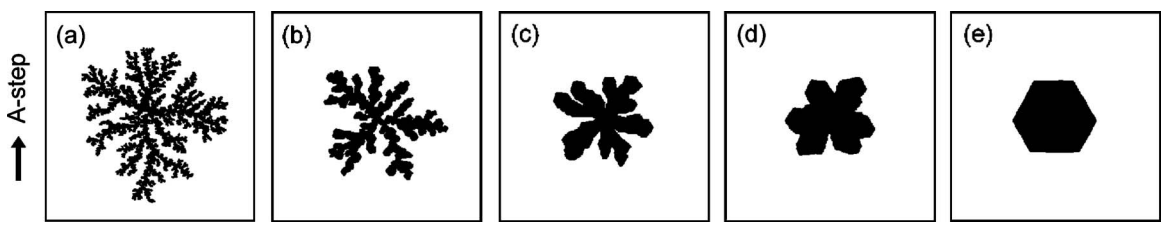

FIG. 8. Images of island shapes (400×460 lattice sites) obtained by Monte Carlo simulations as a function of E_{edge}: (a) 0.80 eV, (b) 0.60 eV, (c) 0.53 eV, (d) 0.48 eV, and (e) 0.35 eV. The number of atoms is 20 000. Calculations were performed under the condition of $E_t=0.010$ eV, $E_{ca}=E_{cb}=0.11$ eV, $T=300$ K and $F=1\times10^{-3}$ ML s^{-1}. The arrow in the figure denotes the direction perpendicular to the A step.

$E_{edge}=0.35$ eV. The island shown in Fig. 8(d) seems to have a partly hexagonal contour and resemble the second-layer islands on Pt [Fig. 2(b)] and the fifth-layer islands on Ir [Fig. 1(c)]. It is emphasized that our simulations well reproduce the island shapes observed on each layer in our STM measurements.

V. DISCUSSION

A. Island density

According to a mean-field theory, the density of the island formed during the growth under constant temperature and flux is proportional to $\nu_t^{-i/(i+2)}$,[25] where i is the critical island size. The critical island size implies that islands consisting of $i+1$ or more atoms are stable. The power-law exponents obtained from the curves fitted to the simulation data shown in Fig. 6 are -0.38 for no corner diffusion (broken line, $i=1$) and -0.52 for $\nu_t=\nu_c$ (solid line, $i=2$). These values are in reasonable agreement with the mean-field theory. The slightly smaller values than the theoretical expectation might be due to the presence of the step which acts as a trap site for adatoms. Furthermore, the fractal growth would make the exponent smaller,[32] since widely spread branches of the dendritic islands capture more adatoms than the compact islands.

From the STM results, it is clear that the island density depends on the underlying substrate as listed in Table I. Considering the simulation result in Fig. 6, the terrace diffusion rate on Ir is higher than that on Pt at 300 K. The dependence of the terrace diffusion rate on the substrate materials would be intuitively attributed to the difference in the interatomic distance of the substrate. When adatoms having a larger atomic size are adsorbed on a surface having a smaller interatomic distance, they feel a less corrugated potential energy surface and diffuse more easily. Au has a larger atomic size than Pt, and Pt has a larger one than Ir. Therefore, Au atoms diffuse more easily on Ir than on Pt. The higher island density on the first Au layer on Ir than that on bare Ir could be also explained by the difference in the interatomic distance, since the interatomic distance of the first Au layer on Ir would be larger than that of Pt.

It should be noted that the strain in the underlying layer caused by the lattice mismatch might affect the adatom diffusion on terraces. According to previous studies, the terrace diffusion is suppressed on a surface having a dislocation network caused by the strain.[33–35] The dislocation network is reported to act as both a repulsive wall[33–35] and a preferred nucleation site[36] for diffusing adatoms. In the former case, adatoms are repelled from the dislocation line, while in the latter case, the dislocation traps the adatoms more strongly than the ordinary terrace site. In either case, the terrace diffusion is suppressed. With increasing Au layer, the strain within the topmost Au layer becomes smaller. As a result, the dislocation network would disappear[33,34] and the island density would approach the value of Au on Au(111).

B. Island shape

Our STM measurements revealed that the shape of the Au islands depends strongly on the underlying substrate. The first-layer islands on Ir and Pt have a dendritic shape with a triangular envelope. Their branches grow into $\langle\bar{1}\bar{1}2\rangle$ directions, i.e., perpendicular to the A steps, and the islands are bound by the B steps. The second-layer islands on Ir have a triangularly compact shape whose corners are pointing to the $\langle\bar{1}\bar{1}2\rangle$ directions, whereas the third- or higher-layer islands on Ir and the second-layer islands on Pt have an irregularly compact shape. Our simulation based on the DLA model with diffusion along island edges well reproduced these island shapes. Therefore, we conclude from the simulation results that the island compactness is determined by the edge diffusion barrier, and that the island symmetry is determined by the corner diffusion anisotropy. By comparing the simulation results shown in Figs. 7 and 8 with the STM results, E_{edge}'s of Au adatoms on Ir and Pt are 0.58 and 0.50 eV, respectively, and the corner diffusion is anisotropic on both substrates. On the other hand, E_{edge} is as low as 0.30 eV on the Au layers grown on Ir and Pt. The corner diffusion is anisotropic on the first Au layer on Ir, whereas it is isotropic on the second or higher Au layer on Ir and on the first Au layer on Pt.

It should be noted that E_{edge} obtained in the simulations would not be an absolute value, since ν_0, E_{ca}, and E_{cb} would also depend on the underlying substrate. Therefore, E_{edge} obtained from comparison of the experiments with the simulations should be a relative value to these parameters. We also note that the shape of an island is influenced by the existence of other neighboring islands and substrate steps. Although most of the simulations performed on the surface with 400×460 lattice sites produced only one island under our simulation conditions, several islands were formed occasionally due to the dimer formation from two terrace adatoms. These islands are found to have a more compact shape than that of the islands formed solely, when they are close together. When other islands or steps exist around an island, the number of atoms coming to the edge sites of the island per unit time becomes lower. This leads effectively to underestimation of E_{edge} as compared to E_t and F. Therefore, when the island densities are higher, i.e., E_t is higher, or when an island is near the steps, the island shape tends to become more compact. However, if an island is more than 50 nm away from other islands or steps, our simulations revealed that the fractal dimension of the island is virtually unaffected by them, and that only the growing direction of the island branches is affected. These results are consistent with an earlier work.[37] In our STM measurements, the islands are sufficiently separated (50–100 nm or more) from each other and steps. Therefore, we can say that the fractal dimension is hardly affected by the steps and neighboring islands in the present study.

It is known that a randomly ramified shape can be explained by the DLA model.[1] In addition to the randomly ramified structure, the triangular envelope which reflects the threefold symmetry of the fcc(111) substrate is explained by the DLA model with corner diffusion anisotropy.[28,30] If the corner diffusion barriers to the A and B steps are different, the corner atoms tend to diffuse to the more easily accessible step. As a result, the branches of the islands grow preferentially in the perpendicular direction to the step and dendritic

islands with a triangular envelope are formed. On the other hand, it is reported that edge diffusion from twofold coordinated sites plays an important role in the transition from the dendritic to compact islands.[8–12] Our results are consistent with these previous studies. Our simulations including both the corner diffusion anisotropy and the edge diffusion well reproduced the shapes of the dendritic and compact islands observed on each layer.

It must be noted that we did not consider the difference between the edge diffusion barriers along the A and the B steps. The edge diffusion barrier is reported to be generally different between along these steps.[28,38–40] However, our simulations well reproduce the experimental results without including the difference. We think that the corner diffusion anisotropy dominantly determines the anisotropy of the dendritic islands, because the edge diffusion is almost hindered in the dendritic growth. Therefore, we conclude that the corner diffusion anisotropy is the dominant factor for the formation of the dendritic islands with a triangular envelope observed in our STM measurements, and that the edge diffusion anisotropy would additionally contribute to the anisotropy of the shape of the compact islands. The difference in the edge diffusion barrier might be necessary in order to simulate the island shape at high temperatures.

As we discussed on the basis of our STM and simulation results, the corner and edge diffusion barriers depend on the underlying substrate. In the following, we discuss the origin of the difference in the diffusion barriers in terms of the difference in the interatomic distance between Au and the substrate. The mean interatomic distance of bulk Ir and Pt is smaller than that of bulk Au by 6.3 and 4.1%, respectively. Our STM and simulation results indicate that E_{edge} becomes lower when the difference in the interatomic distance of the substrate is smaller. It is reported that Au islands grown on Au(111) have a hexagonally compact shape at 300 K.[41] This result indicates that the edge diffusion barrier of Au on Au(111) is lower than those on Ir and Pt, which is consistent with the above argument. The result of the Au islands grown on Au(111) (Ref. 41) also indicates that the corner diffusion is isotropic. Since the corner diffusion is isotropic on the first Au layer on Pt, the first Au layer on Pt would be already like the Au(111) surface, which is consistent with the previous result.[20] On the other hand, the corner diffusion on the first Au layer on Ir is anisotropic, indicating that the first Au layer on Ir is not like the Au(111) surface yet. Because of the larger difference in the interatomic distance, more Au layers would be needed on Ir than Pt for the top layer to approach the Au(111) surface.

There are some studies which support the idea that the difference in the interatomic distance between the adatom and the substrate atom has a relation with the diffusion barriers along the island edges. It is reported that Au on Ru(0001) (Ref. 4) and Au on Pd(111) (Ref. 21) reveal dendritic growth at room temperature. The difference in the interatomic distance between Au and Ru is almost the same as that between Au and Ir, and the compactness of Au islands on Ru is similar to that of Au on Ir of our STM result. Furthermore, the second-layer islands have a triangular shape and their density is much higher than that of the first-layer islands,[42] which is also very similar to our result of Au on Ir. On the other hand, the difference in the interatomic distance between Au and Pd is smaller than that between Au and Ir, and the island shape is more compact than that of Au islands on Ir.[21] Although the detailed mechanism of how the difference in the interatomic distance affects the diffusion barriers is not clarified at this stage, we think that a change of diffusion path caused by the contraction or expansion of edge atoms[28] due to the difference in the interatomic distance would affect the edge diffusion barrier and corner diffusion anisotropy.

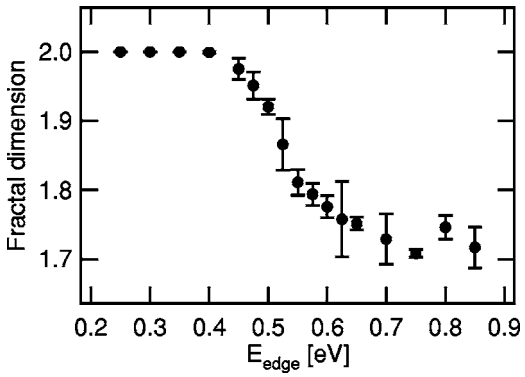

FIG. 9. Fractal dimensions as a function of E_{edge}. Fractal dimensions are measured by the mass-radius relation on the series of simulations shown in Fig. 7.

C. Fractal dimension

The fractal dimensions of the islands obtained in our series of simulations displayed in Fig. 7 are shown in Fig. 9 as a function of E_{edge}. The result clearly shows that the fractal dimension gradually changes from about 1.7 to 2 with decreasing E_{edge}. Such a continuous change of the fractal dimension as a function of the sample temperature has been reported.[8,9,13] It is also reported that the edge diffusion from the twofold coordinated sites plays an important role in the change.[8–12] Nevertheless, implication of the continuous change of the fractal dimension from the viewpoint of statistical physics is not yet fully understood. In the following, we discuss the origin of the gradual change of the fractal dimension.

The fractal dimension is the exponent characterizing a universality class.[43] It is known that there are some universality classes describing film growth such as DLA, ballistic aggregation,[26] and Eden models.[44] The theoretical value of the fractal dimension for the two-dimensional dendritic islands formed by the conventional DLA is reported to be 1.67.[3] The fractal dimension of about 1.7 at high E_{edge}'s in Fig. 9 therefore indicates that the DLA mechanism is operative in this E_{edge} region. As seen in Fig. 9, the fractal dimension at high E_{edge} around 0.80 eV obtained in our simulations is 1.72, which is slightly larger than the theoretical value of 1.67. This slightly higher value is probably due to the effect of random deposition.[45] As the island size becomes larger, the probability of atom deposition on an existing island and between the island branches becomes larger. These events

make the island branches fatter and the fractal dimension larger, even if E_{edge} is sufficiently high to hinder the edge diffusion.

At low E_{edge} around 0.30 eV, on the other hand, the islands have a fractal dimension of 2 as seen in Fig. 9. In this condition, the edge atoms can diffuse along the island edges during the growth. Among the models mentioned above, DLA with edge diffusion has a close relation to the Eden model.[44] In the Eden model, atoms are added to the edge sites of an island one after another with an equal probability at all edge sites. The islands formed under this model are known to be compact and have a fractal dimension of 2.[26] If E_{edge} in our simulations is sufficiently low, the edge atoms can visit many edge sites of an island. Under this condition, all edge sites grow with an equal probability thereby making the island shape like an Eden cluster. Hence, the islands formed at low E_{edge}'s in Fig. 9 should belong to the universality class described by the Eden model.

As discussed above, the islands with fractal dimensions of 1.7 and 2 in Fig. 9 can be described by the DLA and Eden models, respectively. An interesting point is the transition region at $E_{\mathrm{edge}} \sim 0.5$ eV. If the fractal dimension changes gradually, there should be corresponding universality classes. A possible explanation is that this gradual change of the fractal dimension might be caused by the crossover from the DLA to the Eden model due to a finite size effect. If this gradual change were a crossover from the DLA to the Eden model, the system size of the simulation would affect the width of the transition region, i.e., the E_{edge} range where d_f has intermediate values between 1.7 and 2. The width of the transition region is expected to become narrower as the island size increases. In order to investigate the size effect, we simulated the island shape by changing the number of island atoms and analyzed its fractal dimension. As mentioned above, the random deposition effect hinders direct comparison of the fractal dimension for different sizes of islands. In order to avoid the random deposition effect, we performed another series of simulations where atoms are released from the perimeter of the system. The diameter of the perimeter is changed according to the island size to avoid multiple island nucleation. This deposition method is usually adopted in the conventional DLA simulations.[1] It can exclude the random deposition effect, since all atoms are deposited far from the island. The fractal dimension obtained by the method for the islands consisting of 2000, 10 000, 20 000 atoms are shown in Fig. 10. The fractal dimension at high E_{edge} around 0.80 eV, where edge diffusion is virtually prohibited, is about 1.68 at all island sizes, which is consistent with the theoretical value of the conventional DLA model. The result also shows that the fractal dimension changes similarly as a function of E_{edge} independent of the island size. In order to analyze the width of the transition region, we tentatively fitted the data to the steplike function in the form of

$$d_f \sim \left[\exp\left(\frac{E_{\mathrm{edge}} - a}{w} \right) + 1 \right]^{-1},$$

where a and w are the center and the width of the transition region, respectively. The obtained widths of the transition region for the islands which consist of 2000, 10 000, and 20 000 atoms are 0.028 ± 0.005, 0.034 ± 0.010, and 0.038 ± 0.009 eV, respectively. Apparently there is little difference in the width of the transition region among these island sizes. Therefore, we conclude that the gradual change of the fractal dimension is not the crossover from the DLA to the Eden model.

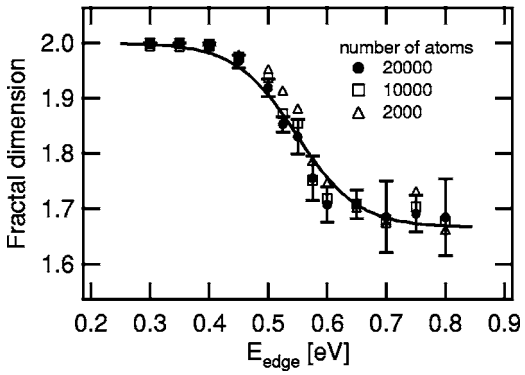

FIG. 10. Fractal dimensions of the islands simulated by the deposition method of the conventional DLA model. Corner diffusion barriers are $E_{ca}=0.10$ eV, $E_{cb}=0.25$ eV. The solid line shows the fractal dimension d_f calculated by $d_f=[4\sqrt{\nu_0 t}\exp(-E_{\mathrm{edge}}/2kT)+5]/[2\sqrt{\nu_0 t}\exp(-E_{\mathrm{edge}}/2kT)+3]$ based on the generalized DLA model (see text) under the condition of $T=300$ K and $\sqrt{\nu_0 t}=6\times 10^4$.

A possible model explaining this gradual change of the fractal dimension is the generalized DLA model.[23,24] The model assumes that the growth probability of an island perimeter site S is proportional to $|\nabla c(S)|^{\eta}$, where $c(S)$ is the probability of finding a randomly diffusing particle at a site S and η is any positive number. It can be proven that the conventional DLA model corresponds to the case of $\eta=1$, and that the Eden model corresponds to the limit of $\eta=0$.[24] According to this model, the fractal dimension d_f is given by $d_f=[d^2+\eta(d_w-1)]/[d+\eta(d_w-1)]$, where d is the Euclidean dimension and d_w is the fractal dimension of trajectories of diffusing particles.[24] Since $d=2$ in two-dimensional island growth and d_w of randomly diffusing particles on a surface is known to be 2,[3] d_f is given by $d_f=(4+\eta)/(2+\eta)$. This equation satisfies both $d_f=1.67$ of the DLA model ($\eta=1$) and $d_f=2$ of the Eden model ($\eta=0$). Furthermore, this equation represents continuous change of the fractal dimension with η. When η is expressed as $\eta=1/m$, this situation can be regarded as the chemical reaction of one randomly diffusing particle with m perimeter sites to be occupied.[24] Following this idea, we consider that m is the average number of edge sites where a diffusing edge atom can attach. Assuming the edge diffusion is one dimensional, m can be written as $m=\sqrt{2D_e t}/a+1=\sqrt{\nu_0 t}\exp(-E_{\mathrm{edge}}/2kT)+1$, where a is the nearest-neighbor distance, D_e is the edge diffusion constant, and t denotes the duration for edge diffusion. The second term on the right-hand side represents an edge site where an edge atom has initially attached, and the first term represents the edge diffusion length from the site. This equation satisfies $m=1$ ($\eta=1$, i.e., DLA model) when E_{edge} is sufficiently high to hinder the edge diffusion. From these equations, d_f is given by

$$d_f = \frac{4\sqrt{\nu_0 t}\exp(-E_{\mathrm{edge}}/2kT) + 5}{2\sqrt{\nu_0 t}\exp(-E_{\mathrm{edge}}/2kT) + 3}.$$

The calculated d_f at $\sqrt{\nu_0 t} = 6 \times 10^4$ and $T = 300$ K is shown in Fig. 10 with a solid line. The curve successfully fits to the simulation results, confirming that the generalized DLA model is an appropriate model for DLA with edge diffusion. The fitting parameter $\sqrt{\nu_0 t} = 6 \times 10^4$ means that $t = 3.6 \times 10^{-4}$ s on the assumption of $\nu_0 = 10^{13}$ s^{-1}. t would be the time needed for edge atoms to diffuse and attach to threefold or higher coordinated sites, or to be stopped by other atoms coming from terraces. t would be determined by the relation among the edge diffusion rate, terrace diffusion rate and flux. The average interval t_f between two successive depositions of atoms can be estimated as $t_f = 9.6 \times 10^{-3}$ s. The time t_a needed for an atom deposited on the terrace to attach an island after diffusion can be estimated to be $\sim 3 \times 10^{-8}$ s. This indicates that deposited atoms usually attach to islands before the next atom is deposited. Hence $t_a \ll t < t_f$, indicating that edge atoms stop before other terrace atoms come to the island edge. The number of edge diffusions that occurred in the simulations, divided by its edge diffusion rate is an order of 10^{-4} s, which is similar to the value t obtained from the fit in Fig. 10. From this analysis, we thus argue that the generalized DLA model is physically satisfactory.

VI. CONCLUSIONS

We investigated the structures of the two-dimensional Au islands grown on Ir(111) and Pt(111) using STM and Monte Carlo simulations. We found that the island shape and island density strongly depend on the substrate. The first-layer islands on both bare substrates have a dendritic shape with a triangular envelope. The second-layer islands have a triangularly compact shape on Ir, whereas the second-layer islands on Pt and the third- or higher-layer islands on Ir have an irregularly compact shape. From the island density on each layer, it is shown that Au atoms on Ir are more mobile than on Pt and on the first-layer Au on Ir. We also found that the fractal dimensions of the dendritic islands are different for growth on Ir and Pt surfaces. Monte Carlo simulations reveal that the fractal dimension of an island is determined by the edge diffusion barrier from twofold coordinated sites of the island edge. Our experimental and simulation results indicate that the edge diffusion barrier depends on the substrate, which is discussed in terms of lattice mismatch between the adlayer and substrate. The simulations also show that the fractal dimension gradually changes from 1.7 to 2 as a function of the diffusion barrier, which well reproduces the experimental results. The gradual change can be explained by the generalized DLA model. We suggest that the generalized DLA model represents the two-dimensional island growth involving adatom edge diffusion.

ACKNOWLEDGMENTS

This work was supported by a Grant-in-Aid for Scientific Research and COE Research from the Ministry of Education, Science, Sports and Culture of Japan. The authors thank M. Matsushita and N. Hatano for useful comments and discussions on the analysis of the fractal dimension.

*Electronic address: ogura@iis.u-tokyo.ac.jp

[1] T. A. Witten and L. M. Sander, Phys. Rev. Lett. **47**, 1400 (1981).
[2] P. Meakin, Phys. Rev. A **27**, 1495 (1983).
[3] K. Honda, H. Toyoki, and M. Matsushita, J. Phys. Soc. Jpn. **55**, 707 (1986).
[4] R. Q. Hwang, J. Schröder, C. Günther, and R. J. Behm, Phys. Rev. Lett. **67**, 3279 (1991).
[5] F. B. de Mongeot, M. Scherer, B. Gleich, E. Kopatzki, and R. J. Behm, Surf. Sci. **411**, 249 (1998).
[6] U. Käsberger and P. Jakob, Surf. Sci. **540**, 76 (2003).
[7] H. Röder, E. Hahn, H. Brune, J.-P. Bucher, and K. Kern, Nature (London) **366**, 141 (1993).
[8] Z. Zhang, X. Chen, and M. G. Lagally, Phys. Rev. Lett. **73**, 1829 (1994).
[9] J. M. Rogowska, Vacuum **74**, 153 (2004).
[10] Y.-Q. Xu, B.-G. Liu, E. G. Wang, and D.-S. Wang, J. Phys. D **34**, 1137 (2001).
[11] S. Ovesson, A. Bogicevic, and B. I. Lundqvist, Phys. Rev. Lett. **83**, 2608 (1999).
[12] M. C. Bartelt and J. W. Evans, Surf. Sci. **314**, L829 (1994).
[13] F. Suda, S. Kawauchi, and M. Ito, Jpn. J. Appl. Phys., Part 1 **42**, 6726 (2003).
[14] G. S. Bales and D. C. Chrzan, Phys. Rev. B **50**, 6057 (1994).
[15] The coordination number in the present paper is given in the in-layer coordination number.
[16] M. Haruta, Catal. Today **36**, 153 (1997).
[17] M. Okada, M. Nakamura, K. Moritani, and T. Kasai, Surf. Sci. **523**, 218 (2003).
[18] M. Okada, K. Moritani, T. Kasai, W. A. Diño, H. Kasai, S. Ogura, M. Wilde, and K. Fukutani, Phys. Rev. B **71**, 033408 (2005).
[19] M. Okada, S. Ogura, W. A. Diño, M. Wilde, K. Fukutani, and T. Kasai, Appl. Surf. Sci. **246**, 68 (2005).
[20] S. Ogura, K. Fukutani, M. Wilde, M. Matsumoto, T. Okano, M. Okada, T. Kasai, and W. A. Diño, Surf. Sci. **566-568**, 755 (2004).
[21] B. Gleich, M. Ruff, and R. J. Behm, Surf. Sci. **386**, 48 (1997).
[22] M. Ruff, S. Frey, B. Gleich, and R. J. Behm, Appl. Phys. A **66**, S513 (1998).
[23] L. Niemeyer, L. Pietronero, and H. J. Wiesmann, Phys. Rev. Lett. **52**, 1033 (1984).
[24] M. Matsushita, K. Honda, H. Toyoki, Y. Hayakawa, and H. Kondo, J. Phys. Soc. Jpn. **55**, 2618 (1986).
[25] J. A. Venables, Philos. Mag. **27**, 697 (1973).
[26] T. Vicsek, *Fractal Growth Phenomena* (World Scientific, Singapore, 1989).
[27] S. C. Wang and G. Ehrlich, Phys. Rev. Lett. **67**, 2509 (1991).
[28] H. Brune, H. Röder, K. Bromann, K. Kern, J. Jacobsen, P. Stoltze, K. Jacobsen, and J. Nørskov, Surf. Sci. **349**, L115 (1996).
[29] J. Jacobsen, K. W. Jacobsen, P. Stoltze, and J. K. Nørskov, Phys.

Rev. Lett. **74**, 2295 (1995).
[30] M. Hohage, M. Bott, M. Morgenstern, Z. Zhang, T. Michely, and G. Comsa, Phys. Rev. Lett. **76**, 2366 (1996).
[31] H. Brune, Surf. Sci. Rep. **31**, 121 (1998).
[32] J. Villain, A. Pimpinelli, L. Tang, and D. Wolf, J. Phys. I **2**, 2107 (1992).
[33] J. A. Meyer, P. Schmid, and R. J. Behm, Phys. Rev. Lett. **74**, 3864 (1995).
[34] H. Brune, K. Bromann, H. Röder, K. Kern, J. Jacobsen, P. Stoltze, K. Jacobsen, and J. Nørskov, Phys. Rev. B **52**, R14380 (1995).
[35] H. Brune, M. Giovannini, K. Bromann, and K. Kern, Nature (London) **394**, 451 (1998).
[36] D. D. Chambliss, R. J. Wilson, and S. Chiang, Phys. Rev. Lett. **66**, 1721 (1991).
[37] K. Sekar, G. Kuri, P. V. Satyam, B. Sundaravel, D. P. Mahapatra, and B. N. Dev, Solid State Commun. **96**, 871 (1995).
[38] T. Michely, M. Hohage, M. Bott, and G. Comsa, Phys. Rev. Lett. **70**, 3943 (1993).
[39] R. Stumpf and M. Scheffler, Phys. Rev. Lett. **72**, 254 (1994).
[40] T.-Y. Fu and T. T. Tsong, Phys. Rev. B **61**, 4511 (2000).
[41] C. A. Lang, M. M. Dovek, J. Nogami, and C. F. Quate, Surf. Sci. **224**, L947 (1989).
[42] R. Q. Hwang, C. Günther, J. Schörder, S. Günther, E. Kopatzki, and R. J. Behm, J. Vac. Sci. Technol. A **10**, 1970 (1992).
[43] A.-L. Barabásy and H. E. Stanley, *Fractal Concepts in Surface Growth* (Cambridge University Press, Cambridge, 1995).
[44] M. Eden, in *Proceedings of the Fourth Berkeley Symposium on Mathematical Statistics and Probability*, edited by J. Neyman (University of California Press, Berkeley, 1961), Vol. IV, p. 223.
[45] T. A. Witten and P. Meakin, Phys. Rev. B **28**, 5632 (1983).